J. Fluid Mech. (1971), *vol.* 47, *part* 1, *pp.* 183–208
Printed in Great Britain

Turbulent air flow over the dominant component of wind-generated water waves

By P. C. CHANG,† E. J. PLATE‡
Colorado State University, Fort Collins, Colorado
AND G. M. HIDY§
National Center for Atmospheric Research, Boulder, Colorado

(Received 1 May 1970)

This paper presents a laboratory study of the dynamic properties of air flow over small wind-generated water waves. On the basis of measurements of mean velocity profiles, turbulent intensity profiles and energy spectra, the detailed structure of turbulent wind immediately above and between the crests of progressive water waves has been examined.

The velocity sensor (a hot-wire anemometer) was fastened to a self-adjusting positioner to measure instantaneous air velocities at a fixed distance from a moving water surface. The waves had a dominant frequency, 2·4 Hz, and a ratio of wave celerity and air friction velocity close to one. With the aid of a digital computer, the desired parameters of air flow were obtained by a statistical technique which was developed to sample and average simultaneous recordings of water surface displacements and instantaneous air velocities.

The results of the wind field measurements over representative waves indicate that, on the average, the air flow separates from the wavy water surface just behind crests, and reattaches somewhere on the windward face of the next wave. The measured turbulent quantities consistently show the characteristics of separated air flow. The separation phenomenon suggests that, without some modification, the Benjamin–Miles shearing flow mechanism is inapplicable to the growth of fully-developed small water waves, at least when the ratio of the phase speed to air friction velocity is of order unity. The observed flow configuration tends to support the separation mechanism of energy transfer originally outlined by Jeffreys and later explored further by Stewart and Deardorff.

Mean properties of the turbulent air flow referred to the mean water level were obtained by continuous sampling of the air flow over many waves with a sensing probe, either at a fixed distance from the mean water level (fixed probe measurement) or at a constant distance from the moving water surface (moving probe measurement). It was found that for continuously averaged measurements, the fixed probe yielded results which deviate less from the local mean than the moving probe results. This holds for the mean velocity distributions and especially for the turbulent quantities.

Present addresses: † University of Utah, Salt Lake City, Utah. ‡ Argonne National Laboratory, Argonne, Illinois. § Science Center, North American Rockwell Corporation, Thousand Oaks, California.

1. Introduction

A combination of circumstances has led recently to a vigorous effort aimed at understanding the interaction between the wind and the underlying sea. On the one hand, there is considerable practical interest in this problem as it relates to broader questions of meteorology and oceanography. On the other hand, the process of generation and growth of wind waves is of basic interest because it involves the stability problem of the interface of a two-phase fluid system. This problem was partially solved theoretically during the 1950's. However, experimental indirect evidence is accumulating pointing to the limitations of the theory, mainly because of unknown interactions between the wind field and waves of which theories do not take account. One of the crucial requirements for an understanding of the nature of these interactions, and thus for further improvement of theoretical ideas, is an exact description of the air flow very near the waves.

Because of the random character of a field of wind-generated waves it might at first sight seem unlikely that such a description can be obtained from experiments. But our own experience in observing the development of wind waves in a laboratory has led us to the conclusion that many important features of the air motion over wind waves arise from its interaction with the principal wave component, or *dominant wave*, and can be identified by statistical mean properties. As shall be shown, the results of this paper fully justify this view.

Wind-generated water waves have a potential energy spectrum whose most striking feature is its pronounced peak, associated with a wave-number k_0, and the sharp decline of spectral density on both sides of the peak. According to Longuet-Higgins (1952), such spectra are indicative of a train of waves of wave-number k_0 with random amplitude modulation, within a pattern of much smaller random waves. Although observed wave patterns generally do not contain an average periodic train of waves, there is no doubt that such a wave train exists in wave groups passing by a fixed point of observation. These persistent, regular waves are the dominant waves, and almost all the variance of the water surface elevation is associated with them. The behaviour of the dominant waves is only little affected by the presence of other wave components and it is therefore possible to apply classical gravity wave theory to them and to describe the increase in potential energy of the waves in terms of the growth of the dominant waves.

Dominant waves generated by a steady uniform wind show different regions of energy transfer depending on the fetch x and the 'wave age' c/u_*, where c is the phase velocity of the dominant wave, and u_* is the shear velocity of the wind blowing over the waves. Except for the waves at very short fetches, the dominant waves in all regions consist of *equilibrium waves*, that is, in it there exists a wave pattern with dominant waves whose magnitude is limited by the acceleration of gravity. The maximum acceleration of the wave is therefore proportional to g, which occurs at the crest of the observed wave. Since the acceleration of the wave crest is proportional to ak, where a is the amplitude and k the wave-number of an infinitesimal gravity wave, it follows that the

dominant equilibrium wave has a constant slope, ak, at least to the order of the validity of infinitesimal gravity wave theory. It was shown by Plate, Chang & Hidy (1969), and independently by Longuet-Higgins (1969), that all wave spectra which have a peak spectral density corresponding to an equilibrium wave have a common envelope described by the -5 power law of Phillips (1958). Also, if the wave pattern consists of equilibrium waves at all frequencies and which do not interact, then this envelope applies to the individual spectrum.

At present, the energy transfer process from wind to equilibrium waves is not completely understood. The theory must account not only for the increase of the potential energy of the wave pattern with fetch, under steady conditions, or with time and fetch for a time-varying wind field, but also for the fact that the frequency of the peak spectral density decreases with increase in fetch or wind speed. It is unlikely that the shift in frequency is associated with selective energy transfer from the wind to the below equilibrium wave components. Experimental evidence (for example, Hidy & Plate 1966) points more to a lengthening and acceleration of some of the dominant waves in a wave train under the action of the wind by a process which is not yet explained. Qualitatively, however, the wind drag evidently forces the waves to absorb more energy, in response to which the waves increase their speed of progression. But the free modes of a water surface wave corresponding to the increased phase speed are of lower wave-number, and consequently the wavelength increases. This sequence of events accounts for the fact that, at least in laboratory conditions, the observed phase speed always slightly exceeds the gravity wave speed $c^2 = g/k$ corresponding to the dominant wave, or its finite amplitude equivalent (Hidy & Plate 1966).

A theoretical model has been given by Deardorff (1967) in which the details of the wave lengthening process were ignored but in which the dominant waves were assumed to be equilibrium waves in the sense used here (although not so identified). This approach was quite successful in predicting the change of the wave variance with fetch under a steady wind as observed in the laboratory and in the field. Deardorff's model, as well as others based on similar assumptions which are reviewed in the paper of Deardorff (1967), can be refined only if more detailed knowledge is available on the wind field near the waves, and such information exists only for wind over solid waves studied in the laboratory (Motzfeld 1937; Stanton, Marshall & Houghton 1932; Bonchkovskaya 1955). These wind-tunnel results are conflicting, however, and those that are available are not likely to be directly applicable to wind–wave interaction, for a number of reasons. For example, the waves chosen were of a shape different from equilibrium water waves. Too few solid waves were used so that the boundary layer for air travelling over the waves was not fully developed, and the boundary layer was too thin compared to the wave heights to yield a useful comparison with field conditions. Besides, recent experiments by Kendall (1970) on the air flow along a boundary consisting of very low amplitude cam-driven waves in a rubber sheet have indicated that the phase velocity of the waves influences the pressure distribution exerted by the air on the waves. Thus, as pointed out some time ago by Ursell (1956), studies of the air flow

over fixed solid waves are of questionable relevance to problems of air–sea interaction.

It now appears that a deeper understanding of wind–wave interaction processes can only be obtained by observing the air-flow distributions over actual wind waves. As a contribution to this goal, we have developed experimental techniques for measuring air velocities with respect to a co-ordinate system fastened to waves. The results of these experiments are presented in this paper. Such data can give some clues as to the structure of the turbulent air flow over small wind waves, and they also should serve as a reference case for comparison with studies of fixed waves.

2. Observational considerations

The properties of air flow over a moving water surface can be observed from several different points of view. We have performed three types of measurements of the air velocity field above progressive water waves. The first type of measurement, which will be called *fixed probe measurement*, is made at a fixed point relative to a fixed reference frame. The height of this point is defined as the average distance above the mean water level. Quantities obtained for this case are identified by the subscript f. This is the usual technique which has been employed for most previous measurements over water waves. The second type, which will be called *moving probe measurement*, and denoted by the subscript 0, is made at a point that has a fixed distance from the moving water surface at any instant. These two types of measurements yield overall mean properties of air flow averaged over many waves and thus show the effect of all Fourier components making up the wavy surface. Both pertain to the same mean water level, but the air flows sampled in them yield different air flow properties at the same average height from the mean water level.

The third type of measurement, which will be called *short time local measurement*, is made at a point that has a definite position with respect to the crest of a particular wave. The local properties of the air flow are obtained from data taken with the moving probe. The measurements consist of simultaneous records of air velocity, probe position and water surface elevation as a function of time. From them, local values are obtained which are associated with the reference frame fixed to the wave by suitable identification and averaging techniques. Local averages are formed over times which are short compared with the period of the wave, but which are long compared to the characteristic time scale of the turbulent dissipation.

2.1. *Velocities obtained from moving probe experiments*

An orthogonal Cartesian co-ordinate system (x, y, z) will be used to specify the positions in the physical space, where x is the fetch or the longitudinal distance measured along the downstream direction, y is the distance along the vertical direction taken upwards from the mean water level, and z is the distance along the lateral direction. For the measurements taken with respect to the moving

water surface, the distance from the point of measurement to the moving water surface is defined as ξ. The velocity components are (u, v, w).

The instantaneous velocity of air in the direction of wave propagation as obtained by a moving probe consists of a time mean $\overline{u}_0$, a random component due to turbulence u_0', and a velocity component $\hat{u}_0$, due to inviscid streamline displacement and due to mean velocity variation along the path of the probe. Thus,

$$u(x, \xi, z, t) = \overline{u}_0(x, \xi, z) + u_0'(x, \xi, z, t) + \hat{u}_0(x, \xi, z, t). \tag{1}$$

Here the quantity $\hat{u}_0$ is highly correlated with the wave motion and is assumed to be statistically independent of the turbulence component u_0'.

If a hot-wire probe is used as a sensing element in moving probe measurements, and if the vertical distance travelled by the probe is denoted by $p(t)$, the velocity sensed by the wire held normal to the mean flow is

$$\mathbf{u}_0 = (\overline{u}_0 + u_0' + \hat{u}_0)\,\mathbf{i} + (v_0' + \hat{v}_0 + dp/dt)\,\mathbf{j}, \tag{2}$$

or

$$|\mathbf{u}_0| = [\overline{u}_0 + u_0' + \hat{u}_0)^2 + (v_0' + \hat{v}_0 + dp/dt)^2]^{\frac{1}{2}}, \tag{3}$$

where dp/dt is the probe velocity which is the rate of change of water surface elevation at the given point.

If $(\overline{u}_0 + \hat{u}_0) \gg \hat{v}_0, u_0', v_0', dp/dt$, this expression can be approximated by the binomial expansion with high-order terms neglected,

$$|\mathbf{u}_0| = |\overline{u}_0 + u_0' + \hat{u}_0|. \tag{4}$$

From (4) the mean velocity $\overline{u}_0$, and the measured root-mean-square of velocity fluctuations $[\overline{u_{0m}'^2}]^{\frac{1}{2}}$ obtained from continuous sampling by use of a hot wire at a fixed distance from the moving water surface, are found equal to

$$\overline{u}_0(x, \xi, z) = \lim_{T \to \infty} \frac{1}{2T} \int_{-T}^{T} u_0(x, \xi, z, t)\, dt \tag{5}$$

and

$$\begin{aligned} [\overline{u_{0m}'^2}]^{\frac{1}{2}} &= \{[\overline{(\overline{u}_0 + \hat{u}_0 + u_0') - \overline{u}_0}]^2\}^{\frac{1}{2}} \\ &= [\overline{\hat{u}_0^2} + \overline{u_0'^2}]^{\frac{1}{2}} \end{aligned} \tag{6}$$

since $\overline{\hat{u}_0 u'} \equiv 0$ according to assumption. Consequently, in the stationary time series given by a sample record of moving probe measurements the $\hat{u}_0$ component will contribute both to the turbulent intensity and the spectral density distribution.

The turbulence can be separated from the measured quantity by correlating the components of the velocity $u_{0m}' = u_0' + \hat{u}_0$ with a simultaneously obtained wave record, provided that the fluctuation $\hat{u}_0$ is linearly related to the water surface undulation η, because by definition the turbulent velocity u_0' is not correlated with the surface undulation. It can be shown that the true turbulent component $\overline{u_0'^2}$ can be estimated from

$$\overline{u_0'^2} = \overline{u_{0m}'^2} - \overline{\hat{u}_0^2} = (1 - R_{u_0 \eta}^2)\, \overline{u_{0m}'^2}, \tag{7}$$

where $R_{u_0 \eta}$ is the correlation coefficient between wave motion and the fluctuating air velocity. It denotes that fraction of the measured turbulent intensity at a

point that is proportional to and in phase with the wave and probe motions, and it is defined as

$$R_{u_0\eta} = \frac{\overline{u_0\eta}}{[\overline{(\hat{u}_0+u_0')^2}]^{\frac{1}{2}}[\overline{\eta^2}]^{\frac{1}{2}}}. \tag{8}$$

Similarly, if the linear relation between $\hat{u}_0$ and η is extended to every Fourier component, the turbulent energy spectrum $S_{u_0'u_0'}(f)$ can be separated from the apparent spectrum $S_{u_{0m}'u_{0m}'}(f)$ by the relation

$$S_{u_0'u_0'}(f) = [1 - Coh_{u_0\eta}(f)]\, S_{u_{0m}'u_{0m}'}(f). \tag{9}$$

Here the coherency $Coh_{u_0\eta}(f)$ denotes that fraction of measured turbulent energy which is associated with the wave and probe motions at a certain frequency. It is defined as

$$Coh_{u_0\eta}(f) = \frac{[S_{u_{0m}'\eta}(f)]^2}{S_{u_{0m}'u_{0m}'}(f)\, S_{\eta\eta}(f)}. \tag{10}$$

2.2. *Observation of local air flow properties*

The water surface is composed of a great number of waves which are different in size, shape and velocity. Therefore, local characteristics of the air flow over any particular wave have little statistical significance. But with respect to an average dominant wave, an associated velocity field can be defined. Individual waves of the 'dominant' class deviate only slightly from a mean dominant wave, and the mean of the ensemble of these waves can be found by well-known statistical methods, applied, for example, to a sample of the n highest waves in a recording of water surface displacement. These waves may be identified in the record, and the associated velocity field can be obtained from simultaneous wave and velocity records. The detailed procedure is described below.

2.3. *Average dominant waves*

An average dominant wave is obtained from a sufficient number n of the highest waves which are picked from the wave record by scanning the wave peaks. The peaks of these highest waves are then aligned at the same reference abscissa, and averaging of the ordinate values yields the average dominant wave. Formally, this process corresponds to a convolution of the water surface elevation $\eta(t)$ with the Dirac delta function $\delta(t)$ whose origin is the time T_{pi} of passage of the peak of each chosen wave, as measured by a wave gauge. The average dominant wave, $\langle\eta\rangle$, is then obtained from the averaging process

$$\langle\eta\rangle(T_p \pm j\Delta t) = \frac{1}{n}\sum_{i=1}^{n}\int_0^T \eta(t)\,\delta(T_{pi} \pm j\Delta t)\,dt, \tag{11}$$

where T is the duration of the wave record, Δt is the spacing of data points obtained in the process of digitizing the wave record. The angular brackets indicate the ensemble averages defined as

$$\langle\eta\rangle = (1/n)\sum_n \eta_n, \quad \text{and} \quad j = 0, 1, 2, \ldots, q,$$

q is so chosen that $q\Delta t$ is larger than a period of the dominant wave.

The resulting lowest average points on both sides of the peak are then defined as troughs, and the distance between them is defined as the average period. The average frequency, the reciprocal of the average period, is equal to the frequency of the dominant wave and also to the frequency of the spectral peak.

2.4. *Local characteristics of turbulent air flow*

After a sample of dominant waves is obtained and identified in the digital record, the air velocity data corresponding to the chosen waves are determined over a specified time range at various positions above the water waves with respect to their crests, as shown in figure 1. For a short piece of instantaneous velocity record of width $2\Delta t$ indicated in the circular insert into figure 1, the

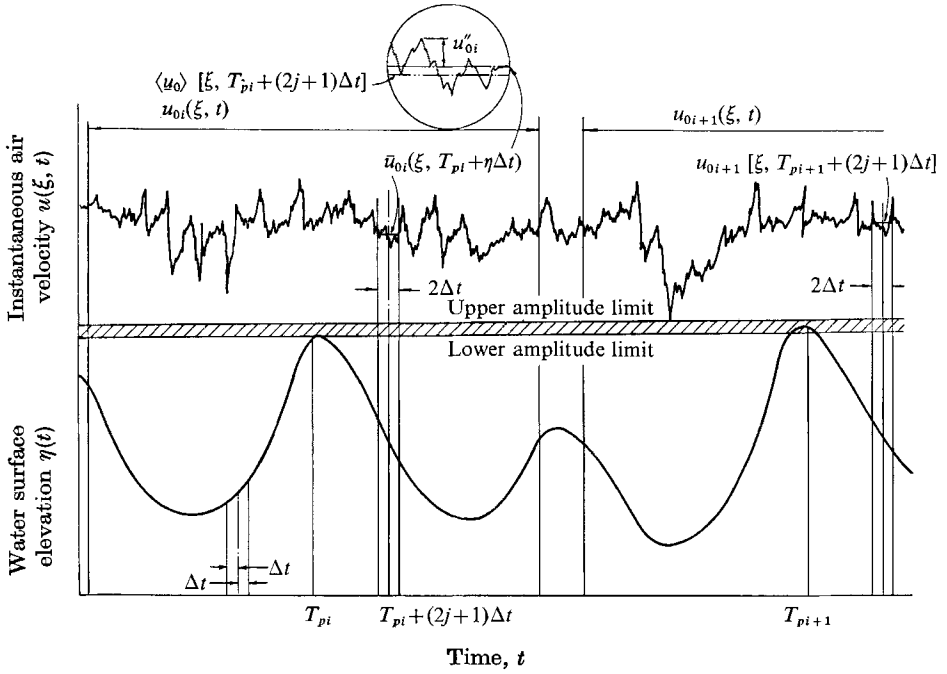

FIGURE 1. Schematic diagram for the procedure of determining average dominant waves and local air velocity properties.

mean, the turbulent intensity and the spectrum can be calculated. The time range $2\Delta t$ for short time averaging should be short enough to yield a local mean velocity in the air. But it should also be long enough to include the fluctuating components in the frequency range of interest. The duration of this time range will be determined in the next section.

The ensemble local mean velocity $\langle \mathbf{u}_0 \rangle [\xi, T_p \pm (2j+1)\Delta t]$, at given points with respect to the peak of average dominant waves is found by averaging over all the selected waves

$$\langle \mathbf{u}_0 \rangle [\xi, T_p \pm (2j+1)\Delta t] = \frac{1}{n} \sum_{i=1}^{n} \frac{1}{2\Delta t} \int_{T_{pi} \pm 2j\Delta t}^{T_{pi} \pm (2j+2)\Delta t} u_{0i}(\xi, t)\, dt$$

$$= \frac{1}{n} \sum_{i=1}^{n} \bar{u}_{0i}[\xi, T_{pi} \pm (2j+1)\Delta t], \tag{12}$$

where $u_{0i}(\xi, t)$ is the instantaneous velocity record corresponding to the ith chosen wave. The time $T_p \pm (2j+1)\Delta t$ refers to the position of the velocity record with respect to the wave peak; it does not imply a 'time' dependence of mean velocity at a certain point. The quantity $\langle \mathbf{u}_0 \rangle [\xi, T_p \pm (2j+1)\Delta t]$ is the velocity at a point (ξ, x) above an average wave.

Each short time-local mean $\bar{u}_{0i}$ may deviate from its ensemble mean $\langle \mathbf{u}_0 \rangle$. A measure of the deviation is the quantity

$$(1/n) \sum_{i=1}^{n} (\bar{u}_{0i} - \langle u_0 \rangle)^2 = \sigma_a^2$$

which will be called the *variance of the short time mean.* If the deviation of the local instantaneous velocity from the short time local mean $\bar{u}_{0i}[\xi, T_{pi} \pm (2j+1)\Delta t]$ is denoted by $u''_{0i}[\xi, T_p \pm (2j+1)\Delta t]$, then the ensemble mean of turbulent kinetic energy of all waves at a point which is fixed with respect to the wave is obtained from the relationship (see figure 1):

$$\begin{aligned} \overline{\langle \mathbf{u}_0'^2 \rangle}[\xi, T_p \pm (2j+1)\Delta t] &= \frac{1}{n} \sum_{i=1}^{n} \frac{1}{2\Delta t} \int_{T_{pi} \pm 2j\Delta t}^{T_{pi} \pm (2j+2)\Delta t} (\bar{u}_{0i} + u''_{0i} - \langle \mathbf{u}_0 \rangle)^2 \, dt \\ &= \overline{u_0''^2}[\xi, T_p \pm (2j+1)\Delta t] + \sigma_a^2[\xi, T_p \pm (2j+1)\Delta t]. \end{aligned} \quad (13)$$

The first term on the right is the average energy of the fluctuating velocities about the short-term local mean and represents the average energy contributed by the high-frequency fluctuations. The second term is the variance of the individual short time means with respect to the ensemble mean, which represents the contribution of the low-frequency components of the velocity field to the kinetic energy.

In a similar manner, the ensemble mean $S_{u_0' u_0'}[f, \xi, T_p \pm (2j+1)\Delta t]$ of the turbulent energy spectrum at a fixed point with respect to the peak of the average dominant wave is obtained from the relation

$$S_{u_0' u_0'}[f, \xi, T_p \pm (2j+1)\Delta t] = \frac{1}{n} \sum_{i=1}^{n} S_{u_{0i}' u_{0i}'}[f, \xi, T_{pi} \pm (2j+1)\Delta t]. \quad (14)$$

Here, $S_{u_{0i}' u_{0i}'}$ is the spectral estimate obtained from a single piece of short time record.

3. Experimental equipment and procedures

The experiments were performed in the wind-wave channel located in the Fluid Dynamics and Diffusion Laboratory of Colorado State University. The facility and the experimental arrangement have been described in detail by Plate (1965). The experimental conditions were set up so that the air velocity field approached the water surface along a smooth flat plate of 5 m length. The fetch x is measured from the end of the smooth plate.

For the purpose of measuring air velocities above the interface of progressing wind waves with a moving probe, a self-adjusting probe positioner was developed.

This device has been described in detail elsewhere (Chang *et al.* 1969). The positioner mainly consisted of a mechanical system and an electronic circuit which allowed a velocity sensor (a hot-wire anemometer, DISA 55 A 01) to always measure velocities at a fixed distance from the water surface within small error limits. It has a negative feed-back control system. The signal from the capacitance wave gauge (CSU Model) is the reference input to the servo system, and the signal from the position potentiometer is its output. The servo system forces the positioner to maintain a preselected distance between the hot-wire probe and the instantaneous water surface at all times. The dynamic calibration of the system indicated that at 2·4 Hz, the frequency of the dominant wave of this study, the frequency response function is flat within better than 5 %, and the phase shift is less than 0·05 π.

During the data collection, the air velocities at a fixed distance from the instantaneous water surface, the water surface elevations, and the position of the moving probe were recorded simultaneously on an Ampex F.M. tape recorder, type FR 1300. The distances of the hot-wire probe from the instantaneous water level were varied in order to map out the mean velocity distributions of the air in the vicinity of the air–water interface. The smallest distance step was 0·25 cm. The lowest elevation above the water which could be obtained with the probe positioner was about 1 cm. Below this height, occasional water droplets began to disturb the hot wire signal.

The continuous analog recordings were digitized with an Analog to Digital Conversion System (Model 751, produced by the Electronic Engineering Company for the National Bureau of Standards, Boulder, Colorado). Three simultaneously recorded signals from hot wire, capacitance probe, and the position potentiometer were digitized in sequence for 2 min at the rate of 1667 points/sec per channel, resulting in 200 000 total data points with 0·0006 sec spacing between points. The magnetic tapes with the digitized data were then analyzed by means of Colorado State University's CDC 6400 digital computer.

In the actual data reduction process, the number n of waves in a sample was chosen as 20, and the time spacing Δt as 0·015 sec. The time range $\Delta t'$ for calculating local air flow properties was $2\Delta t = 0{\cdot}03$ sec. This was equivalent to approximately one-twelfth wave period, and contained 50 digitized data points. The maximum number of lags for local turbulent correlation calculations was chosen as 25, yielding a spectrum with a frequency band from 33·3 to 833·3 Hz. The accuracies of the local ensemble averages of the spectral densities have been estimated by Chang (1968) as better than 20 % for an 80 % confidence band.

The fixed probe measurements of this study mainly served for comparison purposes and for providing consistency checks. For this type of measurement, wind velocity profiles were measured with reference to the mean water level by a Pitot-static tube fixed in space which was connected to an electronic micromanometer (Transonics Equibar Type 120). Fluctuations in the longitudinal component of air velocity were measured with a constant temperature hot-wire anemometer (DISA 55 A 01). The anemometer output was analyzed directly with analog techniques as described in Plate *et al.* (1969).

4. Results and discussion

The experimental investigations performed in this study were restricted to a fixed fetch (3·5 m) where wind-generated waves were fully developed and where the average ratio of wave celerity to air friction velocity is close to one.

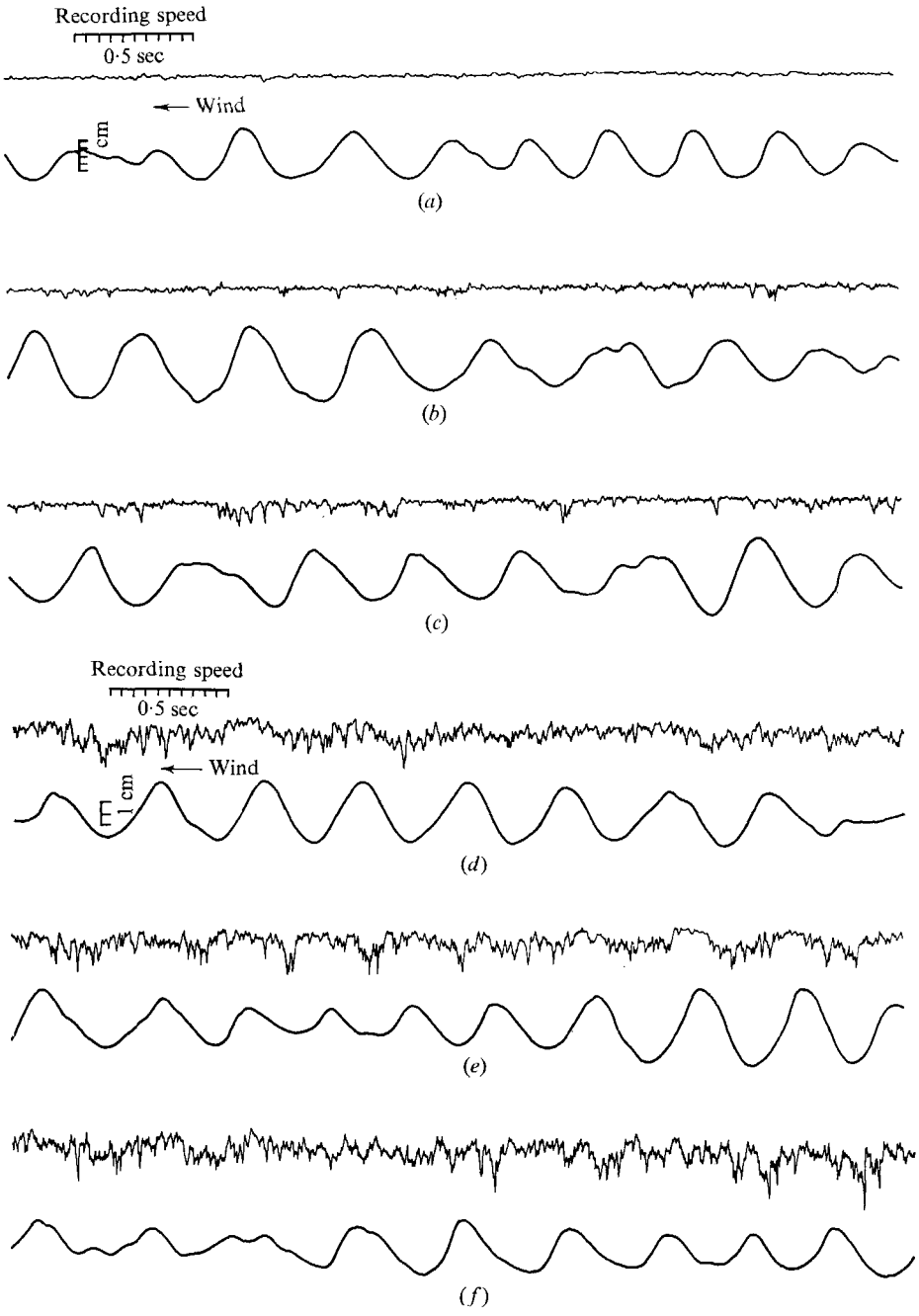

FIGURE 2(*a*)–(*f*). For legend see facing page.

At this stage of growth, only wave components with spectral densities lower than the limit denoted by Phillips's (1958) equilibrium curve tend to increase with fetch so that the wave spectrum is maintained near equilibrium in the high-frequency range of the spectrum. For these conditions, a sequence of simultaneous records of water-surface displacement and instantaneous air velocity as functions of distance from the moving water surface is shown in figure 2. The data were recorded with the d.c. level removed and with arbitrary but constant amplification so that only the instantaneous velocity fluctuations are brought out.

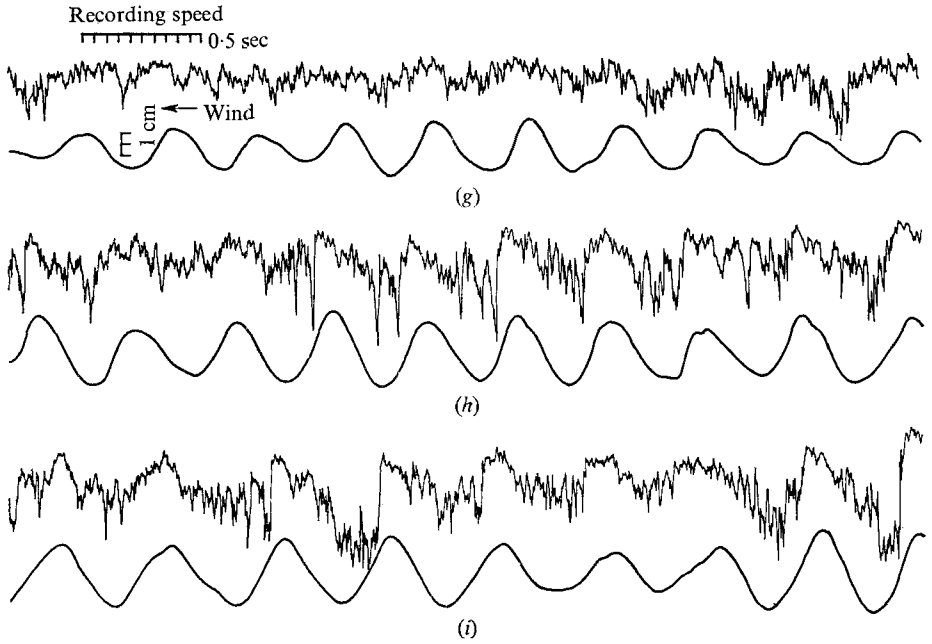

FIGURE 2. Simultaneous records of water waves and turbulent air at a fixed distance from the moving water surface. (*a*) $\xi = 9{\cdot}70$ cm, $\bar{u}_0 = 11{\cdot}32$ m/sec. (*b*) $\xi = 6{\cdot}70$ cm, $\bar{u}_0 = 10{\cdot}62$ m/sec. (*c*) $\xi = 4{\cdot}70$ cm, $\bar{u}_0 = 9{\cdot}50$ m/sec. (*d*) $\xi = 3{\cdot}50$ cm, $\bar{u}_0 = 8{\cdot}85$ m/sec. (*e*) $\xi = 2{\cdot}40$ cm, $\bar{u}_0 = 7{\cdot}90$ m/sec. (*f*) $\xi = 1{\cdot}70$ cm, $\bar{u}_0 = 6{\cdot}52$ m/sec. (*g*) $\xi = 1{\cdot}10$ cm, $\bar{u}_0 = 4{\cdot}7$ m/sec. (*h*) $\xi = 0{\cdot}80$ cm, $\bar{u}_0 = 3{\cdot}8$ m/sec. (*i*) $\xi = 0{\cdot}60$ cm, $\bar{u}_0 = 3{\cdot}02$ m/sec.

At a height well above the air–water interface (about four times the wave height of 2 cm) the air flow is completely free from the effect of water-surface motion (figure 2(*a*), (*b*)) and is characterized by weak irregular oscillations of locally constant intensity. As the measuring probe is moved closer to the water surface, the velocity fluctuations become larger, particularly above wave troughs. The instantaneous velocitybegins to reveal its dependence on the relative position with respect to the wave crest. The local mean velocity above crests is higher than that above troughs (figure 2(*c*)–(*e*)). The dependence of the turbulence on the waves is especially evident in the air flow over higher amplitude waves in the wave train. The air velocity field at smaller distances above the water surface begins to be coupled to the waves, and as the surface is approached the influence of the waves becomes more pronounced. Near the water surface the air flow

shows larger velocity fluctuations just behind the crests, where the air velocity reaches a maximum value and then decreases rapidly further downwind (figure 2(*f*)–(*i*)). The instantaneous velocity directly behind the crest is apparently lower than that in front of the corresponding crest. The observations of figure 2 make it clear that in order to draw meaningful conclusions about the interdependence of air and waves, it is necessary to define local averages with respect to location above a reference wave, i.e. the average of a particular set of statistically similar waves. This is the reason why we selected as our reference wave the average of the 20 highest waves, or the average dominant wave.

4.1. *Average dominant waves*

The statistical properties of the water surface, such as probability distributions, and frequency spectra for wind-generated waves at conditions similar to the ones of this study have been discussed by Hess, Hidy & Plate (1969). There is

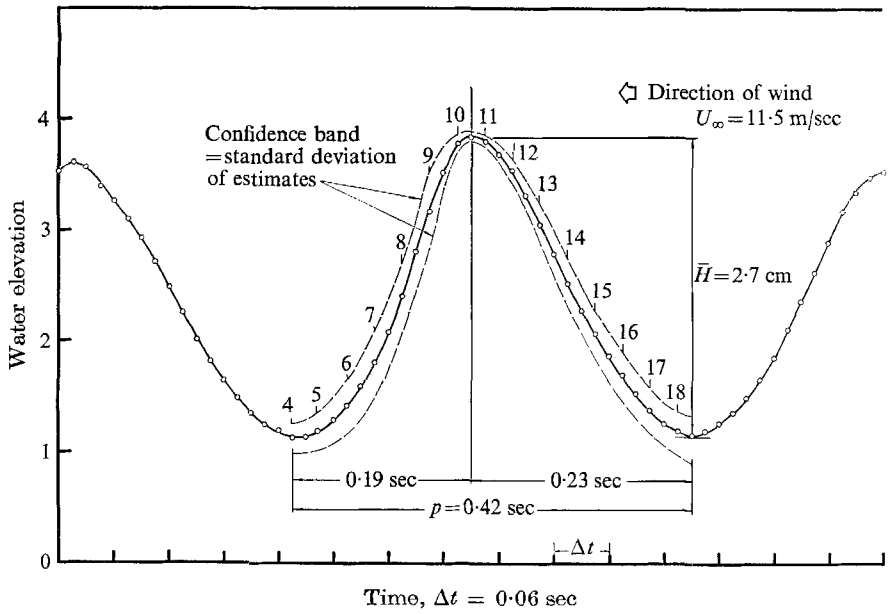

FIGURE 3. Average dominant wave.

no need to reproduce these results because for the purpose of this study the only important water–surface characteristic is the average dominant wave above which local properties of air flow are to be investigated. The average dominant wave obtained by the techniques of §3 is shown in figure 3. Drawn above and below the average wave shape is a curve denoting the local standard deviation of all the 20 waves from the mean, to give an indication of the accuracy of the wave form estimate. The numbers along the waves designate the positions of local averages which are identified by their position i and distance ξ.

The average levels of the troughs on windward and leeward sides of waves are almost identical even though they correspond to different sets of averaged

values. Their elevations are represented by a mean value. The average wave had the following characteristics: the height $\bar{H}$ is 2·7 cm where $\bar{H}$ is the vertical distance from crest to trough, the average wave period $\bar{p}$ is 0·42 sec as measured between windward trough and leeward trough. The average frequency, which is the reciprocal of the average period, equals 2·4 Hz. This value is identical to the dominant frequency associated with the peak of the observed wave-energy spectrum. The wavelength λ calculated from the period $\bar{p}$ by means of the relation between wave period and wave-number obtained from deep-water gravity theory is equal to 27·3 cm, so that the wave steepness $\bar{H}/\lambda$ is equal to 0·1. This value agrees with a mean wave slope given by Sverdrup & Munk (1947), and is slightly larger than the one used by Deardorff (1967) in his model. The wave is strongly skewed, showing a steeper leeward face than windward slope. The ratio of the windward to leeward distance from crest to trough is 1·25. The steeper lee side seems to favour separation of the air flow near the crest.

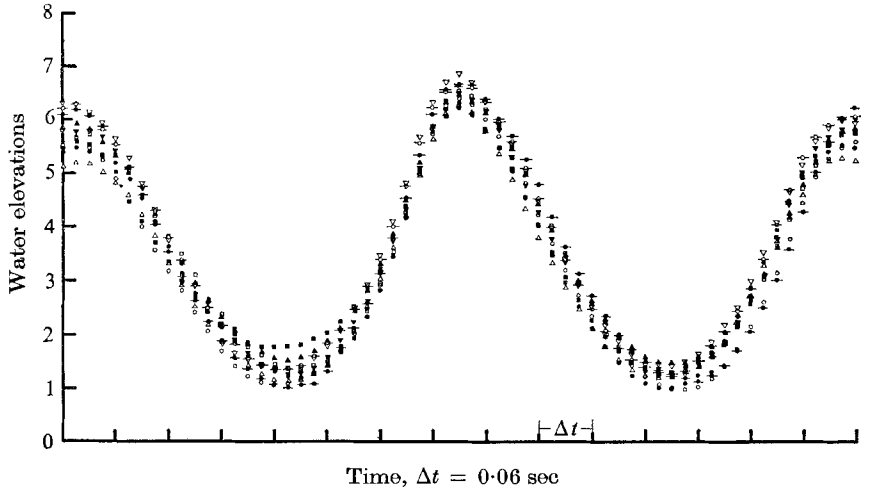

FIGURE 4. A set of average dominant waves. Case 2, run number: —○—, 41; —●—, 43; ○, 46; ●, 47; △, 50; ▲, 51; ▽, 61; ▼, 64; □, 66; ■, 69.

The notably smooth appearance of the average wave is to some extent deceptive. All small ripples have been averaged out. However, their influence is retained in the air flow properties, because the air velocity data were taken before the averaging process for obtaining average dominant waves was applied.

The average waves calculated from the results of different runs are considered to be the same. Ten average waves corresponding to different runs are superimposed in figure 4. The only differences result from the different d.c. levels of the capacitance probe.

4.2. *Mean velocities*

Local mean velocity profiles. The local short time mean velocity is the sum of the overall time mean value and the slowly varying components associated with wave and probe motions. The local short time mean averaged at 14 positions over the wave sample yields the velocity profiles along an average dominant

wave shown in figure 5. These profiles are constructed at the corresponding positions with zero velocity axes vertically through the points they represent. The air-flow direction in the figure is from right to left.

At the lowest elevations, the signal at the lee side of waves was occasionally disturbed by water droplets. Data for which that happened were rejected. In figure 5, two velocity profiles with different symbols are shown at the lowest trough position (position 4 or position 18). They were estimated independently by using the data for the troughs on the windward side and lee side. But they actually represent the same position with respect to the wave, thus illustrating the excellent consistency of the data.

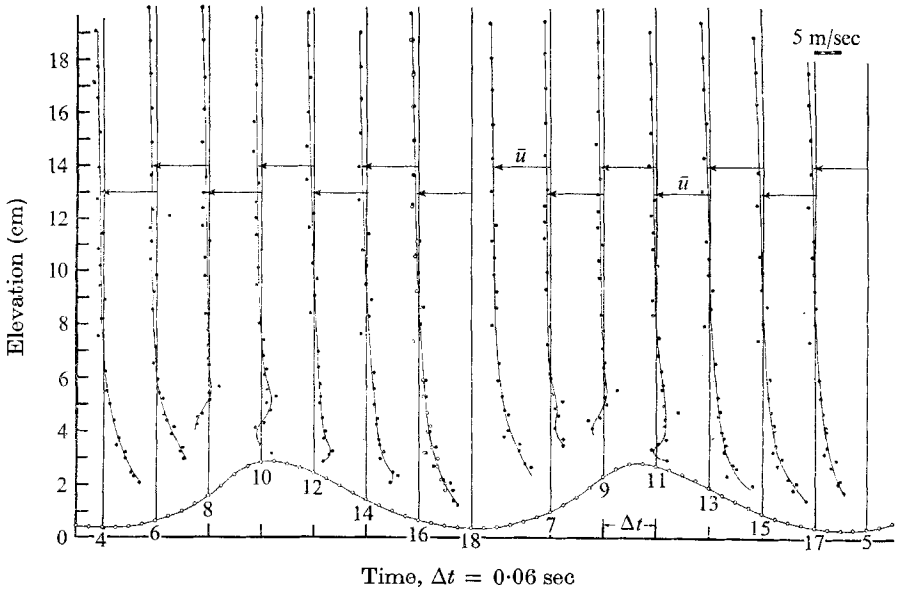

FIGURE 5. Local mean velocity profiles.

The air-velocity profiles are plotted over average dominant waves which are assumed stationary. This is not exactly true since the air–water interface is a more complicated boundary than a solid boundary because of (*a*) the presence of moving waves, (*b*) water particle motions due to the waves, and (*c*) wind-driven drift currents. The apparent mean air velocities would therefore be modified if they were plotted against a co-ordinate system moving with the wave celerity in which the wave profile becomes stationary. However, the phase velocity and water particle velocity are much smaller than the smallest measured air velocity. The critical height where air velocity equals the phase speed of the surface wave occurs on the average in the viscous sublayer of the air flow. Thus these corrections are not significant for interpreting the results.

With a single hot-wire probe as a sensor, only the magnitude of the velocity vector could be measured. Hence, the measured quantities had to be corrected for the angle of attack to yield the velocity in the direction of wave propagation. The velocity profiles shown have a correction for flow direction which was

estimated from the streamline pattern. The construction of streamlines will be described in the next section. The angle correction was important only in the air layer close to the air–water interface.

The results shown in figure 5 clearly indicate that the mean velocity profiles at heights lower than one wave amplitude from the crests are substantially different from position to position above the water waves. A strong 'jet' flow is observed near the wave crests, which is most pronounced at a short distance behind the wave crests. Its maximum velocity can exceed the free-stream value.

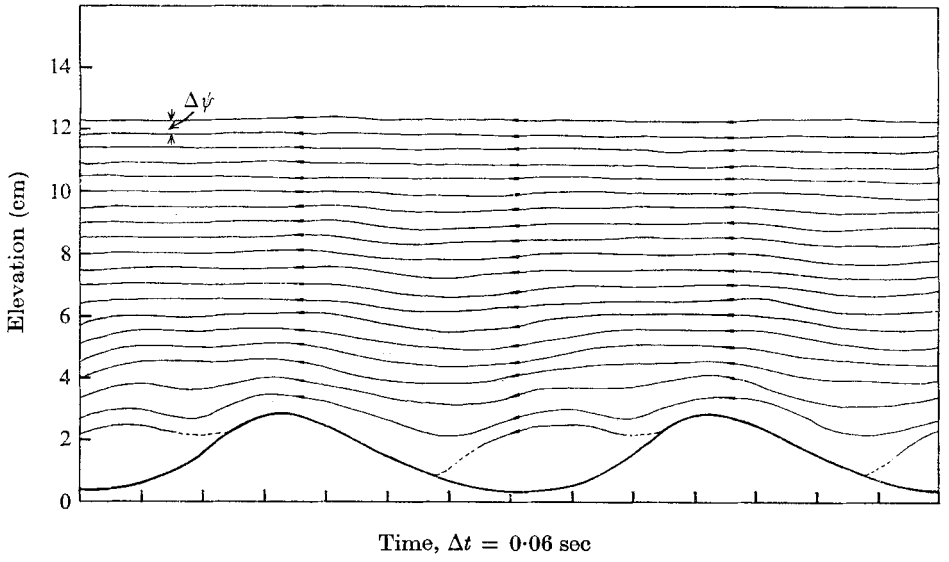

FIGURE 6. Streamline pattern over wind-generated waves. $\Delta\psi$ = 0·043 m³/sec.

Separation and the streamline pattern. Since the flow pattern near the air–water interface was not known, a horizontal line at a height y' equal to four times the wave height, was selected as a reference streamline. At this height, the velocity is free from the effect of surface undulation and is parallel to the mean water level. From this highest streamline additional streamlines were calculated in the usual manner, by first assuming that the measured velocity was the longitudinal component. The streamlines evaluated from this approximation yield an estimate of the inclination of the velocity vector from which the horizontal velocities could be determined for the second approximation. With these values the streamlines were once more determined, and the resulting horizontal velocities compared with those of the second approximation. They were found to be in close agreement.

A typical streamline pattern obtained by this technique is shown in figure 6. The streamlines were constructed as if the boundary were stationary. The results indicate the presence of a stationary eddy or a separated region behind the wave crests, signified by the branching of the lowest streamline from a line just behind the crests. The construction of the streamline pattern in the separated region was not attempted due to insufficient data in this region.

Since the averaged air flow separates from the wave crests and the velocity profiles referred to the instantaneous water surface are substantially different from position to position, the flow configuration differs completely from that assumed in many theoretical investigations for wave growth. In particular, these results illustrate that Miles's (1957, 1962) models cannot be applied rigorously to the growth of small wind-generated waves where $c/u_* \approx 1$. The appearance of flow separation may also explain why attempts to correlate laboratory data with Miles's theory, as attempted by Hamada (1966), Hidy & Plate (1966), Snyder & Cox (1966) and Bole & Hsu (1967), have failed. It was found that the Miles theory systematically underestimates the input of energy from air to water compared with observed rates of growth. Instead, the data support a separation model with a 'sheltering' or drag coefficient which in its earliest form has been proposed by Jeffreys (1925), and of which Deardorff's (1967) model is a more refined version. The observed flow pattern also appears to correspond to the one postulated recently by Stewart (1967).

In generalizing the present results, one may anticipate that air-flow separation occurs at least intermittently over equilibrium waves in the range where $c \approx u_*$. An extension of the present measurements to equilibrium waves at larger values of c/u_* may lead to an air flow which no longer separates, and the conditions at which this may take place deserve investigation. There also arise some questions on the phenomenon of separation. For water waves with large ratios c/u_*, the conventional definition of separation as occurring at a boundary point where the wall shear stress vanishes, appears to be no longer sufficient when applied to a moving boundary.

Mean velocity profiles with reference to the mean water level. From the instantaneous local velocity data over average dominant waves in figure 5, temporal mean velocities can be inferred by calculating the arithmetical mean of the available local mean velocity data at fixed heights either from the mean water level (constant y's), or from the instantaneous water level (constant ξ's). The results correspond to measurements in fixed probe and moving probe reference frames, respectively. Such results are shown in figure 7 (*b*) and (*c*). The mean velocity profile in the turbulent boundary layer upwind of the water surface is seen in figure 7 (*a*) to be logarithmic with height. A weak kink is observed in the mean velocity profiles over waves for fixed probe measurements (figure 7 (*b*)). The data points for moving probe experiments (figure 7 (*c*)) are comparatively scattered, so that only an arbitrary average curve can be drawn. In figure 7 (*c*), the profiles of fixed probe measurements are also shown for comparison. They are indicated by a dashed curve. Near the edge of the free stream these two sets of data are almost superimposed on each other. Only at heights close to the water surface are differences seen. The mean velocity at a given ξ is about 5 % smaller than the mean velocity at an equivalent y, i.e. at $y = \xi$. Similar results were found for flow over solid wave models by Roll (1949), who compared the results corresponding to fixed probe measurements with hypothetical moving probe measurements based on Motzfeld's (1937) wind-tunnel data of air flows over a solid wave model.

At the same conditions the overall mean velocity profiles were also obtained

directly by continuous sampling of velocities over many different wind waves. The fixed probe measurements were taken with a Pitot-static tube and the moving probe measurements were taken with a hot-wire probe. The profiles constructed by plotting velocities against the logarithm of height above the mean water level are shown in figure 7(*d*) and (*e*). The results agree fairly

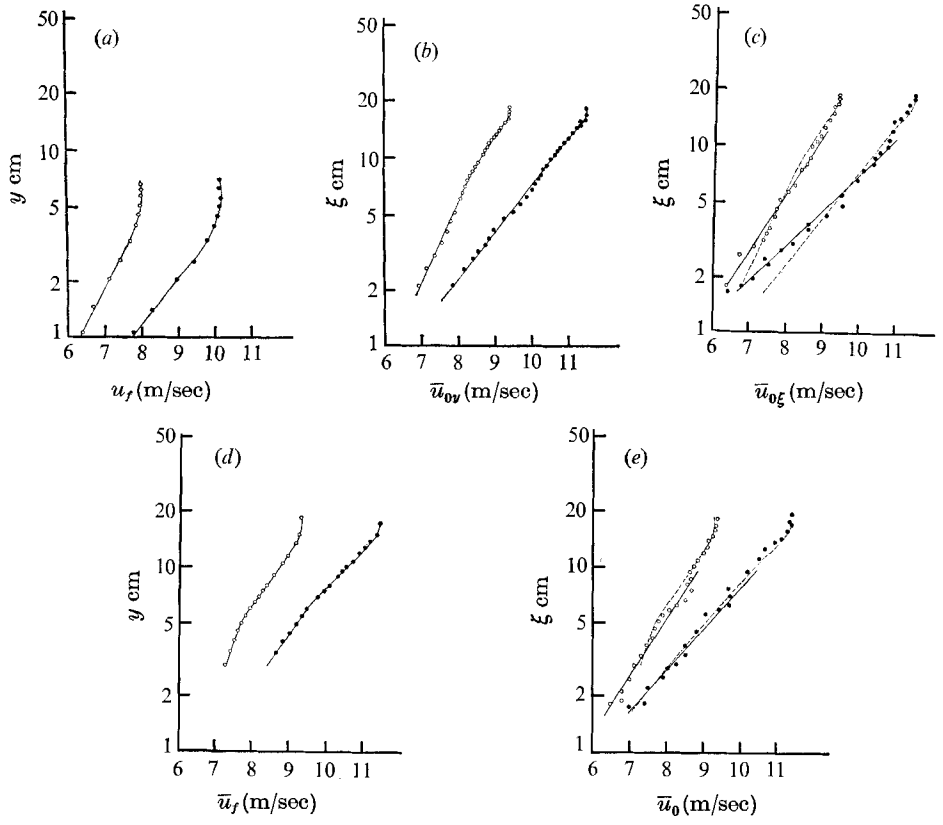

FIGURE 7. Mean velocity profiles above the mean water level. ○, case 1; ●, case 2. (*a*) Mean velocity profile of approaching air flow, x = 45·7 cm. (*b*) Temporal mean velocity profile inferred from local mean velocity data at fixed height from the mean water level, x = 3·5 m. (*c*) Temporal mean velocity profile inferred from local mean velocity data at fixed height from the instantaneous water level, x = 3·5 m. (*d*) Mean velocity profile obtained directly with fixed probe method, x = 3·5 m. (*e*) Mean velocity profile obtained directly with moving probe method, x = 3·5 m.

well with those inferred from the velocity data over the ensemble of the highest waves. Again, at the heights close to the water surface, the data for moving probe measurements are more scattered and show a slightly lower velocity than those obtained by fixed probe measurements; but the difference between the two types of measurement is within experimental error.

The wind profiles obtained from direct fixed probe measurements show the existence of two distinct logarithmic regions (figure 7 (*d*)). The inferred fixed probe measurements exhibit a similar tendency but are not so sharply distinguishable. This result is consistent with observations by Plate & Hidy (1967),

and Shemdin & Hsu (1966), taken over laboratory wind waves; and by Takeda (1963) and Weiler (1966) taken over ocean waves. This feature may be explained in the light of the nature of flow separation. In the presence of separation, the air flow in the separation region is decelerated by a local, adverse pressure gradient. Most of the drag becomes pressure drag, and the skin friction stress becomes smaller than it would have been without separation. Since the shear stress is related to the velocity gradient, the latter is reduced in layers of air close to the surface. At higher elevations, the local pressure gradients are no longer acting and the momentum flux to the wall is supported by the shear stress, and by entrainment of higher velocity fluid at the edge of the boundary layer as in ordinary boundary-layer flows.

4.3. *Turbulent intensity profiles*

Local turbulent intensity profiles. The local $(\langle \overline{u_0'^2} \rangle)^{\frac{1}{2}}$ was calculated from the experiments by means of (13). The profiles of longitudinal turbulent fluctuation at 14 positions along an average dominant wave are shown in figure 8. These

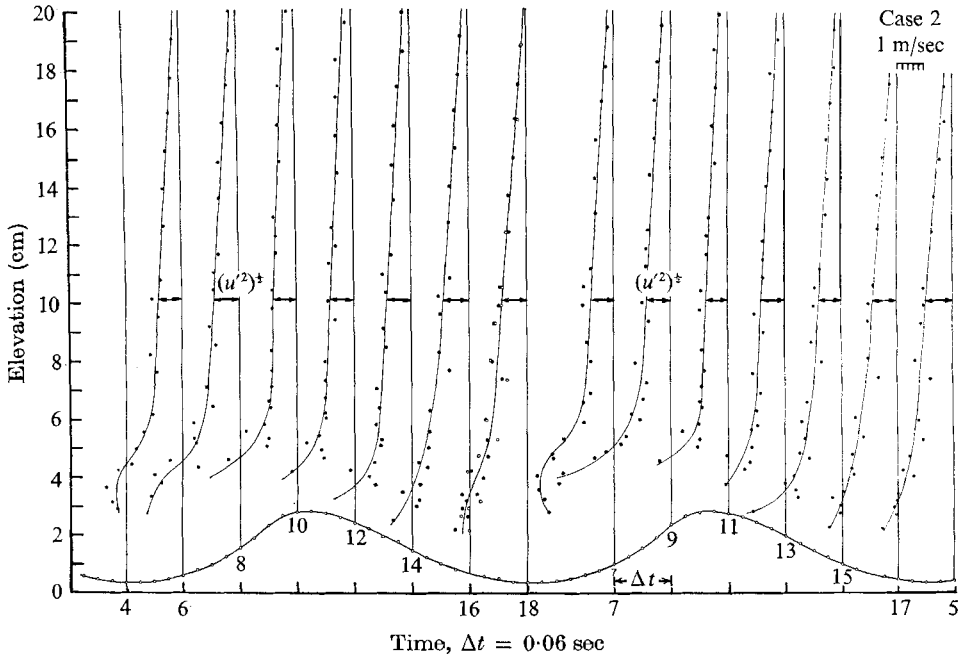

FIGURE 8. Local turbulent intensity profiles.

profiles were constructed at the corresponding positions with zero axes vertically through the points they represent. The direction of the air flow is from the right to left with reference to the figures. Again, two profiles at position 4 and position 18 which correspond to the leeward trough and the windward trough respectively, are expected to be the same since they actually are at the same position with respect to the crests of successive water waves. The superimposed profiles are distinguished by different symbols. They are in satisfactory agreement with

each other. The local $(\overline{u_0'^2})^{\frac{1}{2}}$ profiles indicate that the values of intensities decrease with height. This is characteristic of turbulent shearing flows. When the height is lower than about one wave height from the wave crests, the intensity begins to display a behaviour identified with its dependence on the relative position with respect to the wave crests. A strong maximum in intensity appears at a short distance downstream from the wave crest. This is also the location where the strong jet flow was observed. Downwind of the maximum intensity, the turbulent fluctuation consistently decreases as the air flow moves down to the trough and moves up towards the crest. At the crest, the turbulent intensity in the vicinity of the interface seems to reach its lowest value. This type of turbulent profile is characteristic of the disturbed turbulent flow existing near the streamline which delimits the separation region behind a bluff body, as for example, observed by Arie & Rouse (1956), where the maximum turbulent intensity also occurs near such a streamline.

Longitudinal turbulent intensity profiles with reference to the mean water level. Following the same procedure as used to obtain overall mean velocity profiles, the general turbulent intensity profiles with respect to the mean water level can be constructed from the local turbulent fluctuations above the average dominant waves. Such profiles in fixed probe and moving probe reference frames, $(\langle u_{0y}'^2 \rangle)^{\frac{1}{2}}$ and $(\langle u_{0\xi}'^2 \rangle)^{\frac{1}{2}}$ respectively, are shown in figure 9(*a*) and (*b*). They have been non-dimensionalized with the local friction velocity u_* and were plotted against y/δ, where δ, the boundary-layer thickness, is defined as the height where the mean air velocity is equal to 99 % of the free-stream air velocity. The friction velocity was obtained from the following equation:

$$u_* = 0{\cdot}0185\, u_\infty^{\frac{3}{2}},$$

where u_∞ is the free-stream velocity in m/sec, u_* is given in m/sec. This empirical formula was originally given by Hidy & Plate (1966). They derived this relation from a direct momentum balance involving the average slope of the water surface and the pressure gradient in the air.

The results based on the two reference frames are in perfect agreement. For $y/\delta > 0{\cdot}2$, it seems that the profiles reach an equilibrium shape, since they exhibit a close similarity in shapes to that found in the equilibrium shearing layer of Corrsin & Kistler (1954) whose results for flow over a flat plate roughened by corrugated paper also are shown in figures 9(*a*) and (*b*). For $y/\delta < 0{\cdot}15$, the normalized turbulent intensity significantly exceeds the values found in an equilibrium layer. The scaled profiles of longitudinal fluctuation seem to be similar under equilibrium conditions only at heights greater than the height of the roughness elements, or of the dominant waves.

The results obtained with a fixed probe by continuous sampling over many different wind waves are shown in figure 9(*c*). The fixed probe $(\overline{u_f'^2})^{\frac{1}{2}}$ profiles are consistent with those inferred from the local data over average dominant waves. Unfortunately, because the limitation of the fixed probe technique, the lowest elevation at which data could be taken was at $y/\delta = 0{\cdot}2$, which does not permit a check of the anomalous behaviour that was noticed in the profiles inferred from the local intensity profiles. The average curve of this result is also shown

with a broken line over figures 9 (*a*) and (*b*). The agreement between these results is remarkable.

The moving probe $(\overline{u'^2_{0m}})^{\frac{1}{2}}$ profiles, shown in 9 (*d*), where the subscript $0m$ denotes the uncorrected quantities obtained directly from moving probe measurements, are consistently higher than those obtained directly with the fixed probe.

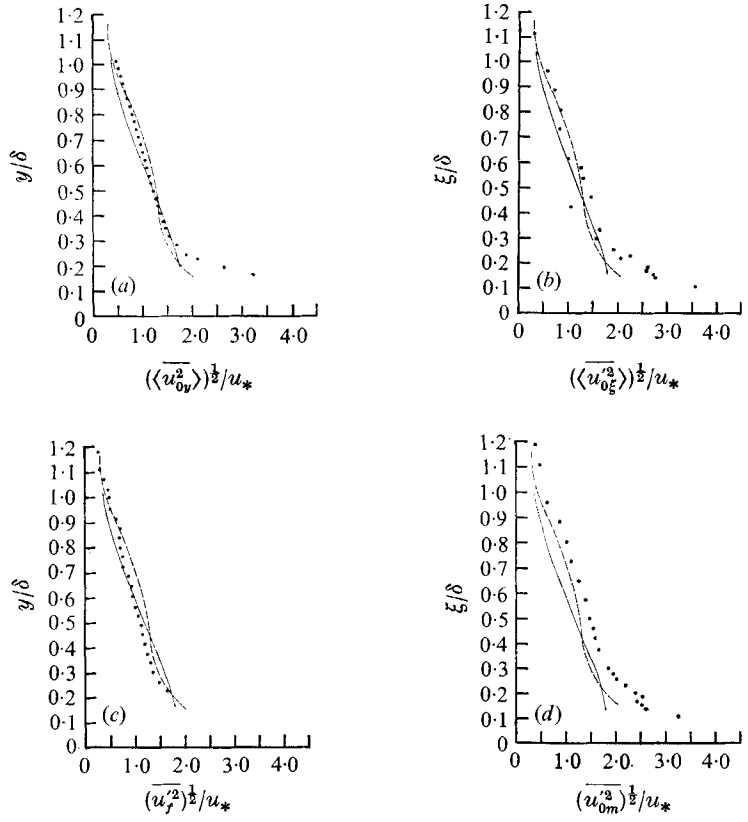

FIGURE 9. Turbulent intensity profiles above the mean water level. ●, this study; ———, Corrsin & Kistler (1954); – – –, corrected profile. (*a*) Turbulent intensity profile inferred from local turbulent intensity data at a fixed distance from the mean water level. (*b*) Turbulent intensity profile inferred from local turbulent intensity data at a fixed distance from the instantaneous water level. (*c*) Turbulent intensity profile obtained directly with fixed probe method. (*d*) Apparent turbulent intensity profile obtained with moving probe method. These data are the sum of true turbulent energy and the contribution from probe and wave motions. Dashed curve is the corrected profile obtained by removing the contribution from probe and wave motions.

This results from the fact that the measured turbulent energy obtained with a moving probe through continuous sampling is the sum of fixed point turbulent energy and the contribution from probe and wave motions. By applying (7), the fixed point turbulent r.m.s. value can be determined from the measured value, $(\overline{u'^2_{0m}})^{\frac{1}{2}}$, and the correlation coefficient $R_{u_0\eta}$. The results are shown with a solid line in 9 (*d*). The corrected moving probe turbulent intensities are close to

the fixed point profile, although they are still generally some 5% higher than inferred values. The difference can be attributed to the non-linear relation between air motion and water displacement.

4.4. *Turbulent energy spectra*

A set of ensemble average spectra for various heights and positions with respect to the crests of average dominant waves are shown in figure 10. The positions of the spectra are identified in the figure. It is remarkable that almost all short-time

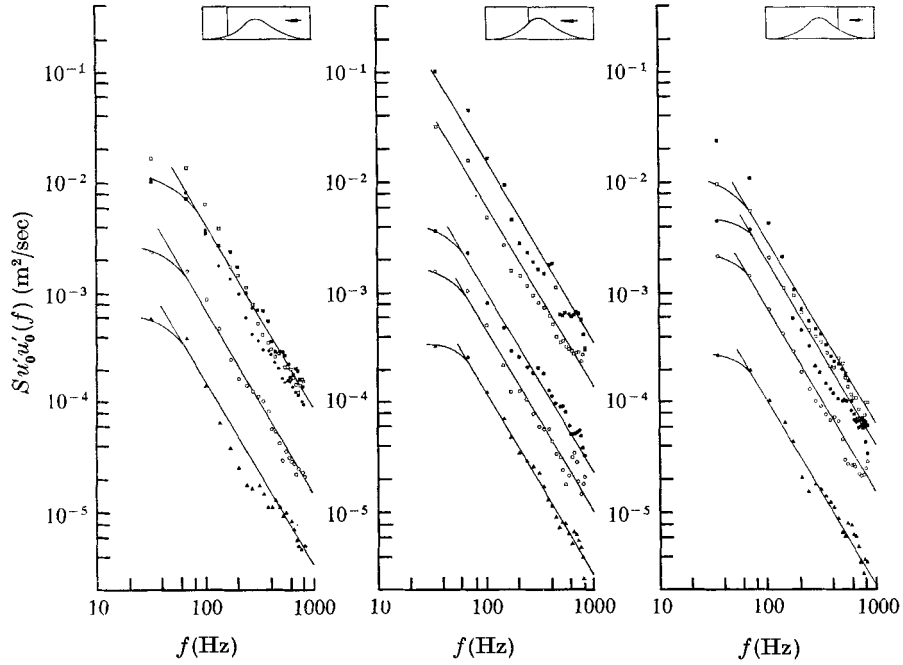

FIGURE 10. Local turbulent energy spectra. Several spectra at wave crest trough and in between are shown. ξ in cm: ▲, 17; ○, 10.8; ●, 4·4; □, 2.3; ■, 1·8.

spectra decrease according to the Kolmogoroff $-\frac{5}{3}$ power law over their whole frequency range. This is seen by comparing the data with the solid lines which are the best fitting curves with a slope of $-\frac{5}{3}$ in the double logarithmic plots of the spectra. This behaviour may be associated with the relatively high Reynolds number of the flow (Hinze 1959, p. 586), and the strong mixing of air caused by the water surface undulation, so that the turbulence rapidly approaches local isotropy.

The energy spectra of the longitudinal velocity fluctuations over all waves were determined from magnetic tape recordings of the hot wire signal. By combining the results from analog spectrum analyzers and from the digital computer, a frequency domain from 1 Hz to 7 kHz was obtained. In figure 11 are shown the energy spectra of longitudinal velocity fluctuations from fixed probe measurements, i.e. turbulent energy spectra. These spectra are still in arbitrary

analog units. All spectra indicate the existence of a viscous dissipation region varying approximately as f^{-7} at the high-frequency range which evolves into the inertial subrange varying as $f^{-\frac{5}{3}}$ with decreasing frequency. The results

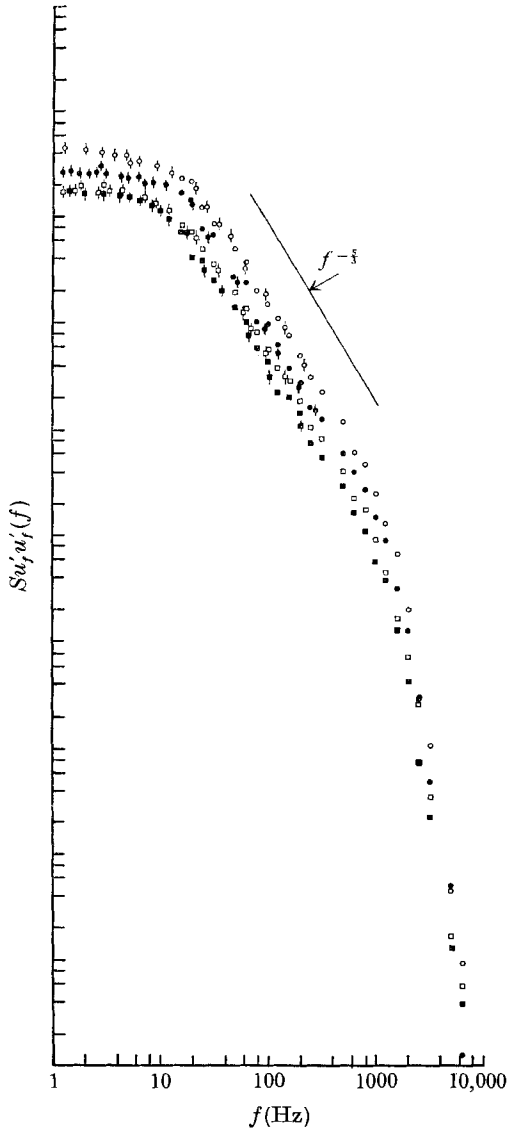

FIGURE 11. Turbulent energy spectrum measured with a fixed probe. Proportional band width, B. & K. spectrum analyzer, y in cm: ■, 11·4; □, 8·91; ●, 6·35; ○, 3·81. Constant band width, Technical Products spectrum analyzer, y in cm: ▮, 11·4; ▯, 8·91; ⬮, 6·35; ⬭, 3·81.

indicate that as noted earlier, for example, by Hinze (1959) the width of the inertial subrange increases with increasing air velocity or local Reynolds number. The spectra do not show an increase in energy near the frequency of the dominant wave which might be attributed to the wave motion. This is in part

due to the fact that measurements with the fixed probe cannot be made close enough to the interface to observe such an energy maximum. Also, the band width of 2 Hz of the analog filter may be too wide to detect a spectral peak around 2–3 Hz.

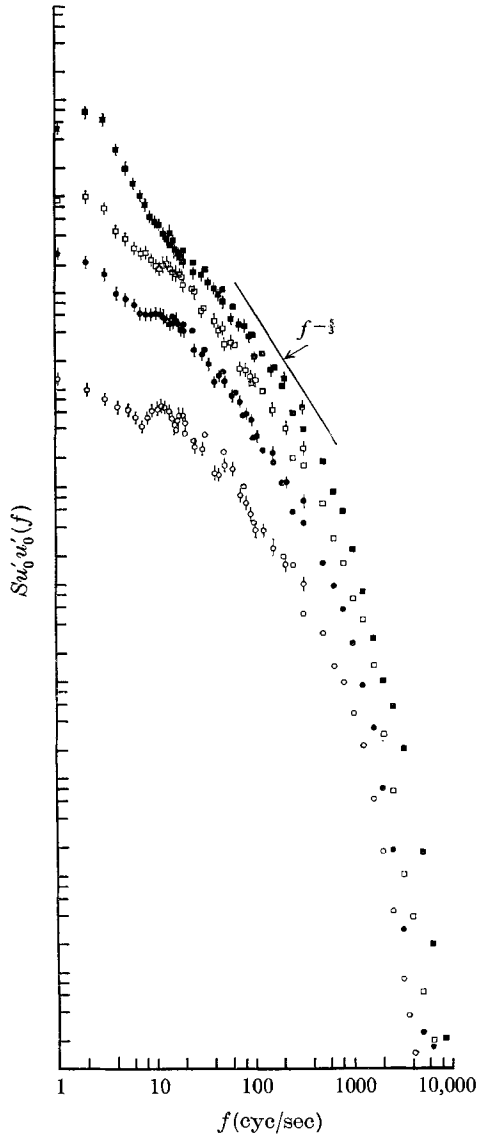

FIGURE 12. Turbulent energy spectrum measured with a moving probe. Proportional band width, B. & K. spectrum analyzer, ξ in cm: ○, 6·74; ●, 4·24; □, 1·71; ■, 0·71. CDC 6400 digital computer, ξ in cm: ⏀, 6·74; ⧳, 4·24; ⏃, 1·71; ▮, 0·71.

Turbulent energy spectra from moving probe measurements are shown in figure 12. Since the probe followed the waves the spectrum of the component $\hat{u}_0$ is added to the spectral density of the spectrum of true turbulence. This component, however, should make its largest contribution near the dominant

frequency of the water-wave spectrum, and thus should cause a distortion of the air-velocity spectrum only at the low-frequency end. The shape of spectrum at frequencies, say, higher than 20 Hz should remain substantially unaltered, and should reveal the same characteristics of a 'pure' turbulent spectrum. As the experimental spectra show, this is indeed the case.

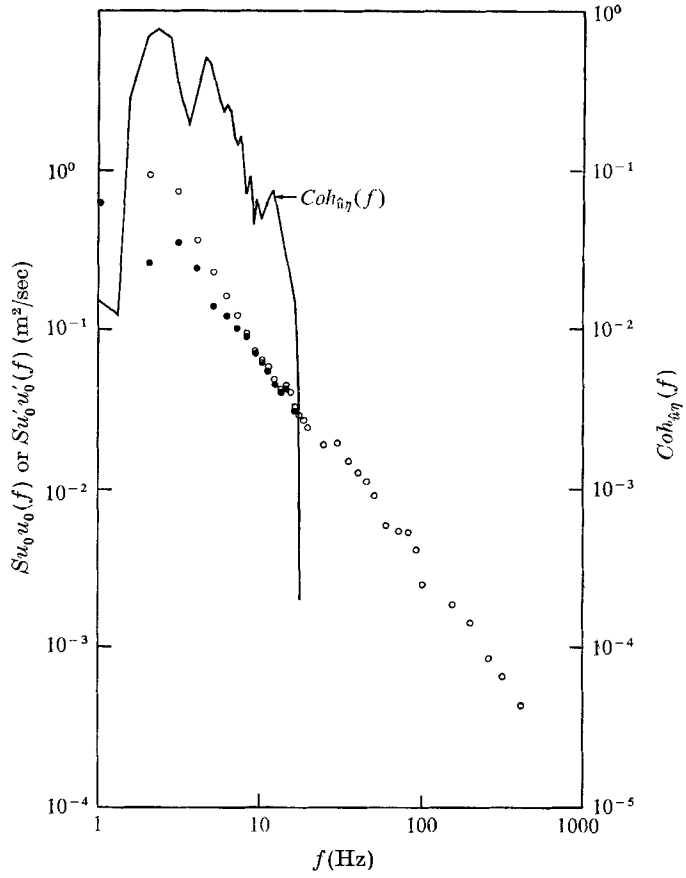

FIGURE 13. Turbulent energy spectrum corrected for wave-probe induced fluctuations. Uncorrected spectrum: ○, $Su_0u_0(f)$; Corrected spectrum: ●, $Su_0'u_0'(f)$: $(1-Coh_{\hat{u}\eta})$ $Su_0u_0(f)$.

At elevations close to the water surface, the motion of the probe and the water surface significantly distort the spectra and a peak appears at the frequency corresponding to the dominant wave near 2·4 Hz. At larger heights from the water surface, the distortion still can be found, but the energy distributes itself more uniformly over the low-frequency end and no energy peak directly associated with dominant wave frequency can be discerned. This rules out the possibility that the peak is due to the probe motion alone, but rather is an indication of the velocity field sampled by the probe during its motion. At the highest position, the contribution from $\hat{u}_0$ seems to be so weak that the whole spectrum reveals only the characteristics of an ordinary turbulent energy spectrum over fixed boundary.

By applying the linear correlation method outlined in §2, the turbulent spectrum has been estimated from moving probe measurements. The result is shown in figure 13. The uncorrected spectrum is denoted by open circles and the corrected spectrum is denoted by solid circles. Comparing the corrected spectrum with that obtained with a fixed probe, it seems that the technique can only correct for the component of the dominant wave peak. The correction to the other low-frequency components is apparently too small.

5. Conclusion

This investigation represents a first direct attempt to measure the detailed structure of turbulent air flow above and between crests of progressing wind-generated water waves. The experiments indicated that indeed meaningful results can be deduced about the wind field averaged over a physically identifiable wave, the dominant wave. The study yielded measured profiles of mean velocity which differ significantly from position to position along average dominant waves. They display many characteristics of turbulent air flow over solid bluff bodies, as do the locally measured turbulent intensity profiles. In particular, the streamline pattern indicates that, at least for the dominant waves in this study, there is no question that a separation region exists. On the average, the air flow separates from the water surface a short distance behind the crest and reattaches somewhere on the windward face of the next wave. The observed flow configuration suggests that the well-known mechanism for wave growth by shearing air flow proposed, for example, by Miles needs re-examination for its applicability to prediction of the growth of fully-developed small water waves where $u_* \approx c$. Instead, the experimental results tend to support the assumed flow configurations proposed in models like those of Jeffreys (1925), Stewart (1967) and Deardorff (1967).

This study also showed the feasibility of using a self-adjusting positioner for observing the local properties of air in the vicinity of the air–water interface. In principle, the technique developed can readily be applied to measurements of pressure or shear stress distributions above and around progressive wind waves, if a fast response pressure sensor or a crossed hot-wire anemometer is attached on the self-adjusting positioner. Similar techniques could also be applied to the surface layer in the water. Such measurements should greatly aid the understanding of the mechanics of air–water interaction.

This work was sponsored in part by the National Science Foundation through its grants GK-188 and 2142 to Colorado State University, and through its contract with the National Center for Atmospheric Research.

REFERENCES

ARIE, M. & ROUSE, H. 1956 *J. Fluid Mech.* **1**, 129.

BOLE, J. B. & HSU, E. Y. 1967 *Stanford University, Dept. of Civil Eng., Tech. Rep.* no. 79.

BONCHKOVSKAYA, T. V. 1955 *Akademia Nauk SSSR, Movskoi Gidrofizicheskii Institute*, **6**, 98.

CHANG, P. C. 1968 Unpublished Ph.D. Dissertation, Colorado State University, Fort Collins, Colorado.

CHANG, P. C., GOROVE, A., ATCHLEY, B. & PLATE, E. J. 1970 *Rev. Sci. Instrum.* **41**, 1544.

CORRSIN, S. & KISTLER, A. L. 1954 *NACA T. N.* 3133.

DEARDORFF, J. W. 1967 *J. Ocean. Soc. Japan*, **23**, 278.

HAMADA, T. 1966 *Port and Harbour Tech. Res. Inst., Rep.* no. 2. Japan: Yokosuka.

HESS, G. D., HIDY, G. M. & PLATE, E. J. 1969 *J. Mar. Res.* **27**, 216.

HIDY, G. M. & PLATE, E. J. 1966 *J. Fluid Mech.* **26**, 651.

HINZE, J. O. 1959 *Turbulence.* New York: McGraw-Hill.

JEFFREYS, H. 1925 *Proc. Roy. Soc.* A **107**, 189.

KENDALL, J. M. 1970 *J. Fluid Mech.* **41**, 259.

LONGUET-HIGGINS, M. S. 1952 *J. Mar. Res.* **11**, 245.

LONGUET-HIGGINS, M. S. 1969 *Proc. Roy. Soc.* A **310**, 151.

MILES, J. W. 1957 *J. Fluid Mech.* **3**, 185.

MILES, J. W. 1962 *J. Fluid Mech.* **13**, 433.

MOTZFELD, H. 1937 *Z. angew. Math. Mech.* **17**, 193.

PHILLIPS, O. M. 1958 *J. Fluid Mech.* **4**, 426.

PLATE, E. J. 1965 *La Houille Blanche*, **6**, 597.

PLATE, E. J., CHANG, P. C. & HIDY, G. M. 1969 *J. Fluid Mech.* **35**, 625.

PLATE, E. J. & HIDY, G. M. 1967 *J. Geophys. Res.* **72**, 4627–4641.

ROLL, H. U. 1949 *Annalen der Meteorologie*, **2**, 71–78.

SHEMDIN, O. H. & HSU, E. Y. 1966 *Stanford University, Dep. of Civil Eng., Tech. Rep.* no. 66.

SNYDER, R. L. & COX, C. S. 1966 *J. Mar. Res.* **24**, 141.

STANTON, T. E., MARSHALL, D. & HOUGHTON, R. 1932 *Proc. Roy. Soc.* A **137**, 283.

STEWART, R. W. 1967 *Phys. Fluids*, **10**, 547.

SVERDRUP, H. V. & MUNK, W. 1947 *U.S. Navy Hydrographic Office Publ.* no. 601.

TAKEDA, A. 1963 *J. Ocean. Soc. Japan*, **19**, 16.

URSELL, F. 1956 In *Survey in Mechanics.* Cambridge University Press.

WEILER, H. S. 1966 Ph.D. Dissertation, University of British Columbia, Vancouver.